Ann. Geophys., 35, 1249–1268, 2017
https://doi.org/10.5194/angeo-35-1249-2017

Annales Geophysicae Open Access EGU

Global characteristics of auroral Hall currents derived from the Swarm constellation: dependences on season and IMF orientation

Tao Huang[1,2], **Hermann Lühr**[2], **and Hui Wang**[1]

[1]Department of Space Physics, College of Electronic Information, Wuhan University, 430072 Wuhan, China
[2]GFZ, German Research Centre for Geosciences, Sect. 2.3 "Geomagnetism", 14473 Potsdam, Germany

Correspondence to: Tao Huang (terence@whu.edu.cn)

Received: 30 November 2016 – Revised: 7 October 2017 – Accepted: 18 October 2017 – Published: 27 November 2017

Abstract. On the basis of field-aligned currents (FACs) and Hall currents derived from high-resolution magnetic field data of the Swarm constellation, the average characteristics of these two current systems in the auroral regions are comprehensively investigated by statistical methods. This is the first study considering both current types determined simultaneously by the same spacecraft in both hemispheres. The FAC distribution, derived from the novel Swarm dual-spacecraft approach, reveals the well-known features of Region 1 (R1) and Region 2 (R2) FACs. At high latitudes, Region 0 (R0) FACs appear on the dayside. Their flow direction, up or down, depends on the orientation of the interplanetary magnetic field (IMF) B_y component. Of particular interest is the distribution of auroral Hall currents. The prominent auroral electrojets are found to be closely controlled by the solar wind input, but we find no dependence of their intensity on the IMF B_y orientation. The eastward electrojet is about 1.5 times stronger in local summer than in winter. Conversely, the westward electrojet shows less dependence on season. As to higher latitudes, part of the electrojet current is closed over the polar cap. Here the seasonal variation of conductivity mainly controls the current density. During local summer of the Northern Hemisphere, there is a clear channeling of return currents over the polar cap. For positive (negative) IMF B_y a dominant eastward (westward) Hall current circuit is formed from the afternoon (morning) electrojet towards the dawn side (dusk side) polar cap return current. The direction of polar cap Hall currents in the noon sector depends directly on the orientation of the IMF B_y. This is true for both signs of the IMF B_z component. Comparable Hall current distributions can be observed in the Southern Hemisphere but for opposite IMF B_y signs. Around the midnight sector the westward substorm electrojet is dominating. As expected, it is highly dependent on magnetic activity, but it shows only little response to season and IMF B_y polarity. An important finding is that all the IMF B_y dependences of FACs and Hall currents practically disappear in the dark winter hemisphere.

Keywords. Ionosphere (auroral ionosphere; ionosphere–magnetosphere interactions; polar ionosphere)

1 Introduction

The ionospheric currents comprise Pedersen current, Hall current, and field-aligned current (FAC). At high latitudes, FACs are important for the energy and momentum transport from the magnetosphere to the ionosphere. The first representative FAC distribution was derived from the magnetometer measurements of the Triad satellite (Iijima and Potemra, 1976a), in which FACs follow a double ring pattern. Region 1 (R1) currents are located on the poleward side, flowing into the ionosphere on the dawn side and out on the dusk side. The Region 2 (R2) FACs are located a few degrees equatorward flowing in the opposite direction to R1 (Iijima and Potemra, 1976b; Juusola et al., 2014; Carter et al., 2016). Previous observations have shown that the interplanetary magnetic field (IMF) orientation has a significant effect on the strength and distribution of FACs (e.g., Weimer, 2001). Most prominent is the influence of the southward IMF component on the current intensity. When IMF B_y is dominant additional FACs poleward of the oval are observed in the noon sector. For example, when IMF $B_y < 0$ ($B_y > 0$) the so-called DPY-related FACs (DPY stands for disturbance polar related to B_y, first introduced by Friis-Christensen and Wilhjelm, 1975) are flowing into (out of) the polar cap in the Northern Hemisphere. This current, more poleward of R1, is named

Region 0 (R0) FAC (Iijima et al., 1978). In the case of northward IMF B_z the so-called NBZ current system dominates the high latitudes in the noon sector (e.g., Vennerstrøm et al., 2002; Wang et al., 2008b). The locations of these IMF B_y-dominated FACs in the noon sector are schematically shown in Fig. 3 of Vennerstrøm et al. (2002).

The Pedersen currents in the ionosphere close the different FACs from the magnetosphere. Their magnetic effects in connection with the FACs are canceling on ground in the case of uniform ionospheric conductivity. The Hall currents are to first-order source-free and close entirely in the ionosphere. However, in cases of significant conductivity gradients, e.g., between the polar cap and auroral zone, the Hall current system contributes also to the closure of field-aligned currents. The magnetic effects of Hall currents can be observed both on ground and in space.

The typical Hall current pattern has a two-cell shape in the high-latitude ionosphere, with a clockwise and counterclockwise flow on the dawn side and dusk side, respectively. At auroral latitudes the electrojets form the main part of the Hall current circuit. They are an important part of the horizontal current system in the ionosphere (Richmond and Kamide, 1988). The distribution of Hall currents in the polar cap region was first determined on the basis of magnetic field data from the International Magnetosphere Study (IMS) Alaska meridian chain (Kamide and Akasofu, 1981). Traditionally, in early studies of Hall currents they were presented in terms of equivalent ionospheric currents because a unique determination of Hall current density is impossible from ground-based magnetic field observations alone. To our knowledge there is no statistical study of the global Hall current distribution derived from satellite data.

In early studies, such as Hughes and Rostoker (1977), the sunward directed return currents over the polar cap were not considered. Therefore net FACs were introduced to feed the electrojets on the dawn and dusk sides. In their model a downward FAC near noon diverges into the westward electrojet past the 06:00 MLT sector and on the afternoon side into the eastward electrojet. When both electrojets reach the poleward boundary of the nightside auroral oval, a conductivity discontinuity drives the electrojet currents upward along the field lines. Today we know that such a current configuration occurs primarily in the winter hemisphere, where the polar region is in darkness (Zhou and Lühr, 2017).

The relationship between high-latitude FACs and the auroral electrojet on the dayside has been studied in many works (Iijima and Potemra, 1976b; Wilhjelm et al., 1978; Senior et al., 1982; Belehaki and Rostoker, 1996), but they are not conclusive. There are different points of view on how to connect the FAC intensity and Hall current properties. A statistical relationship between the orientation of the interplanetary magnetic field and ionospheric currents has been derived from the Greenland magnetometer array (Friis-Christensen et al., 1985). The R0 FAC is considered to be a separate current system, which can vary independently from the electrojets.

The DPY current system, which is controlled by a negative IMF B_y, is regarded by Rostoker (1980) as signature of the redistribution of net downward FACs at local noon. He showed a schematic diagram of DPY currents in his Fig. 8. Belehaki and Rostoker (1996) deduced the actual relationship between DPY currents and ionospheric auroral electrojets with CANOPUS (Canadian Auroral Network for the OPEN Program Unified Study) magnetometer data. The direction of horizontal DPY-related currents across the noon sector at auroral latitudes is strongly dependent on the IMF B_y component. In particular, for $B_y < 0$ ($B_y > 0$) these DPY currents flow toward dawn (dusk) and connect in the prenoon (post-noon) sector to the main westward (eastward) electrojet. We have to note again that the observations mentioned are all based on data from ground-based stations. Therefore, the inferred relationship between Hall current distribution and FAC locations is not unique. Clarifying the situation is one of the goals of this study.

Juusola et al. (2007) are the first to study the three current components (j_r: field-aligned, j_φ: divergence-free, and j_θ: curl-free component) of the ionospheric system simultaneously by means of their 1-D Spherical Elementary Current Systems (SECS) approach based on CHAMP satellite data. They were able to provide a quite detailed description of the current distribution in the dawn and dusk auroral regions. However, near the noon and midnight sectors their 1-D approach did not return reliable results. The ESA constellation mission Swarm provides new opportunities for current density estimate and allows for simultaneously studying the ionospheric FAC and Hall currents in a statistical way.

In the present paper we attempt to take advantage of the Swarm constellation to determine the global statistical characteristics of Hall currents and FACs in different seasons and for different IMF conditions. The results are derived from a period of 3 years (April 2014 to April 2017) of Swarm magnetic field recordings. The Swarm satellite mission and our data set are introduced in Sect. 2. Subsequently, the estimation method for FACs and their average patterns are briefly described in Sect. 3. As mentioned before, the FAC distribution is generally well known. Therefore we focus more on the Hall current distribution in this study. The calculation method and characteristics of Hall currents are presented in detail in Sect. 4. The main findings are discussed in Sect. 5 and compared with previous studies. Finally, we summarize our results in Sect. 6.

2 The Swarm and IMF data sets

The ESA three-satellite Swarm constellation mission (Friis-Christensen et al., 2008) was successfully launched into a near-polar orbit in November 2013 and achieved its final orbit configuration on 17 April 2014. Swarm Alpha (A) and Swarm Charlie (C) fly side by side at an altitude of 460 km and an east–west separation of 1.4° in longitude.

Swarm Bravo (B) is flying at a higher altitude of about 520 km. Swarm A and C can cover all 24 h of local times in about 133 days. The vector field magnetometer (VFM) on board Swarm samples the magnetic field data, and they are routinely calibrated with respect to the Absolute Scalar Magnetometer (ASM). In this study the calibrated Swarm Level-1 and Level-2 magnetic field data are used, which have a time resolution of 1 Hz.

The CHAOS model series, originally derived from the CHAMP, Ørsted and SAC-C satellites, is designed to estimate the global geomagnetic field at near-Earth space with high resolution in time and space. This model includes contributions of the core, crustal, and large-scale magnetospheric fields. It is derived primarily from satellite magnetic field data, but ground-based observations of secular variation are also used. The new version CHAOS-6 (Finlay et al., 2016) also incorporates Swarm data. It is used in this study for deriving the contributions of ionospheric currents to the Swarm magnetic field observations. For this purpose the core, crustal, and magnetospheric field parts of the CHAOS-6 model are subtracted from the actual Swarm A and C field measurements.

For considering the interplanetary magnetic field and solar wind conditions the OMNI database is used, which is publicly available at the Space Physics Data Facility (SPDF) of the NASA Goddard Space Flight Center (http://omniweb.gsfc.nasa.gov). The 1 min resolution IMF data (propagated to the Earth's bow shock as part of the OMNI data processing) are further averaged over 15 min periods. The merging electric field (E_m) is calculated and used as a measure of solar wind input to the ionosphere based on OMNI data, which have been delayed by 20 min allowing for the propagation to the ionosphere (e.g., Vennerstrøm et al., 2002). Making use of the very efficient coupling function introduced by Newell et al. (2007), we calculate the merging electric field as

$$E_\mathrm{m} = \frac{1}{3000} V_\mathrm{sw}^{\frac{4}{3}} \left(\sqrt{B_y^2 + B_z^2}\right)^{\frac{2}{3}} \sin^{\frac{8}{3}}\left(\frac{\theta}{2}\right), \quad (1)$$

where V_sw is the solar wind velocity in units of km s^{-1}, B_y and B_z (in nT) are the IMF components in GSM coordinates, and θ is the clock angle of IMF. When dividing the original Newell coupling function by 3000 the obtained E_m value is in size comparable to the solar wind electric field in mV m^{-1}.

Our study period from 17 April 2014 to 17 April 2017 coincides with the declining phase of solar cycle 24. For the main activity indices we obtain therefore quite moderate mean values but with a fairly large standard deviation: solar radio flux, $F_{10.7} = 111 \pm 40.3$ sfu, geomagnetic activity, $A_\mathrm{p} = 10.5 \pm 9.7$, and merging electric field, $E_\mathrm{m} = 1.31 \pm 1.3$ mV m^{-1}.

3 Distribution of field-aligned currents

3.1 Deriving FACs from Swarm mission

The FAC estimates presented here are based on the advanced Swarm dual-spacecraft technique, as outlined by Ritter et al. (2013). Simultaneous recordings of ionospheric magnetic fields by the spacecraft pair Swarm A and C, flying side by side, are interpreted jointly. Based on Ampère's law in integral form the vertical current density j_z is calculated:

$$j_z = \frac{1}{\mu_0 A} \oint \boldsymbol{B}_\mathrm{H} \cdot \mathrm{d}l, \quad (2)$$

where A is the area encircled by the contour, $\boldsymbol{B}_\mathrm{H}$ is the magnetic field vector in the horizontal plane, dl is the line element along the integration path, and μ_0 is the permeability of free space. In practice the integration, as outlined in Eq. (2), is done in discrete steps. Magnetic field residuals at the four corners, forming a quadrangle, are used in the ring integral. As illustrated in Fig. 1 of Lühr et al. (2015b), two readings are taken along the track, separated by 5 s, of both satellites. When considering the orbital velocity of 7.6 km s^{-1} this corresponds to a distance of 38 km. The cross-track separation between the two satellites is 1.4° in longitude, which amounts to about 50 km at 70° latitude. The result of the integral divided by the encircled area provides the mean vertical current density. In order to avoid spatial and temporal aliasing of the sparsely sampled current distribution, the residual magnetic fields employed here are low-pass-filtered with a 3 dB cutoff period of 20 s corresponding to a wavelength of about 150 km. This eliminates contributions from small-scale FACs, which typically show a lot of temporal variability (Lühr et al., 2015a). Finally, the field-aligned currents $j_{||}$ are obtained by mapping the vertical currents j_z onto the main field direction:

$$j_{||} = \frac{j_z}{\sin(\mathrm{incl})}, \quad (3)$$

where incl is the magnetic field inclination. FACs flowing into (out of) the ionosphere have negative (positive) values in the following sections. Here we have to note that the signs of the inclination are flipped in the Southern Hemisphere such that upward FACs are positive in both hemispheres. More details of the dual-spacecraft FAC estimation technique employed can be found in the article of Ritter et al. (2013). Near the orbital crossover of Swarm A and Swarm C, at 87.3° GLAT, the separation between the spacecraft becomes too small for a reliable dual-satellite FAC determination. Therefore no FACs are determined at latitudes beyond 86° GLAT. In the Northern Hemisphere the omission zone lies within the polar cap, but in the Southern Hemisphere it partly overlaps with the auroral region. The resulting FAC data are sorted into equal-area bins of 330 km × 350 km. The number of samples in each bin, depending on magnetic latitude, is presented in the Supplement for both hemispheres (see Fig. S1).

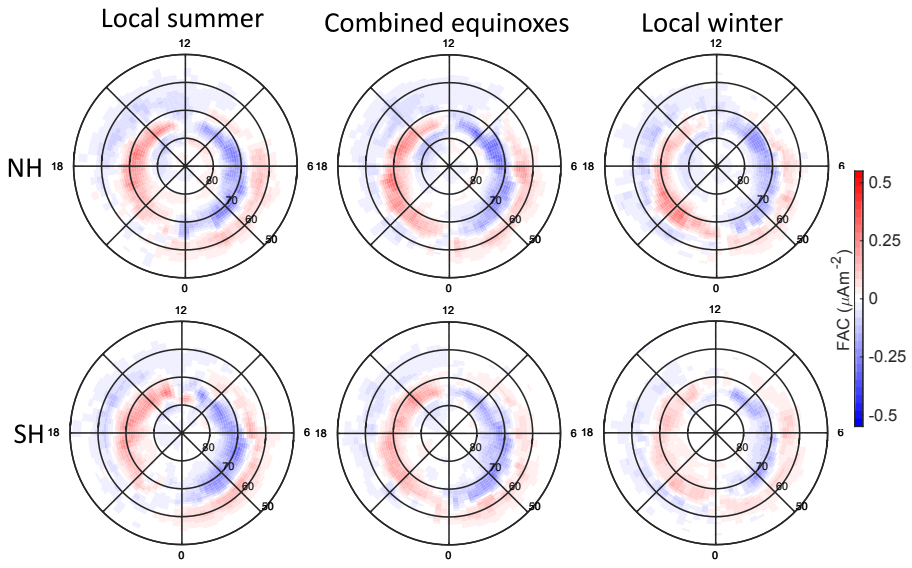

Figure 1. Average distribution of auroral field-aligned currents in the two hemispheres for different seasons. Red colors represent upward currents and blue downward.

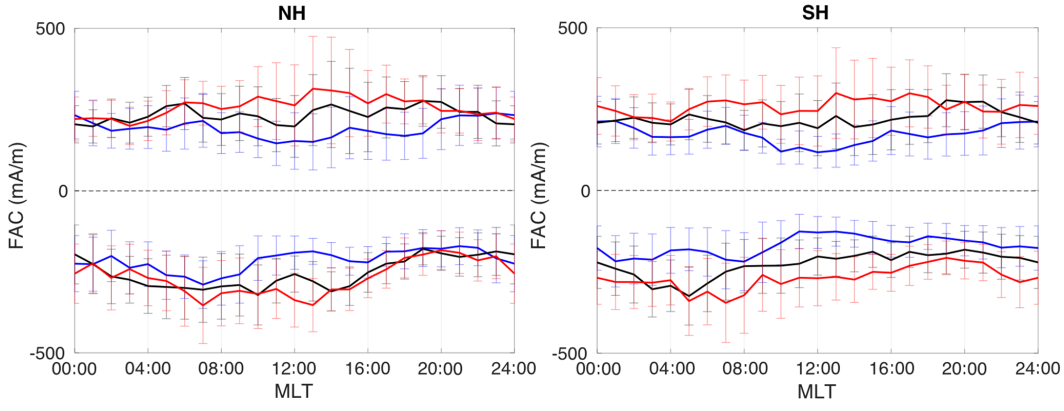

Figure 2. Diurnal variation of averaged FACs in 1 h local time bins for different seasons. The left (right) panels are for Northern (Southern) Hemisphere. The blue, black, and red lines represent local winter, equinox, and summer, respectively. Presented are the summed upward and downward FAC sheet current densities in each hour bin.

3.2 Dependence of FACs on season and IMF

From each Swarm orbit we obtain a latitude profile of FAC density. Combining many orbits provides a map of the FAC distribution. We first have a look at the seasonal dependence and separate the data into three defined periods: June (1 July $\pm$ 66 days) and December (1 January $\pm$ 66 days) solstices and combined equinoxes (1 April $\pm$ 33 days plus 1 October $\pm$ 33 days). The Swarm satellites need just 133 days to cover all local times; therefore these slightly overlapping periods have been chosen. Figure 1 shows the average FAC distributions of the 3 years considered, separately for the two hemispheres. Here we apply the equal-area binning procedure that was introduced for thermospheric wind studies by Lühr et al. (2007). The high-latitude region centered on the magnetic pole is divided into 13 concentric rings, with a 3° MLAT width. The innermost ring (88.5–85.5° MLAT) is subdivided into six sectors and all subsequent rings into $N \times 6$ bins of approximate 330 km $\times$ 350 km size, where N is the sequence number of rings. This provides a latitude-dependent local time resolution ($4/N$ in hours) for the various rings. The measurements are sorted into the bins according to their orbital positions (in MLAT and MLT coordinates) and then statistically averaged. The well-known patterns of R1 and R2 FAC belts appear, and average seasonal differences are most prominent on the dayside. To show the seasonal variation of FAC intensity clearer, for the three seasons FAC sheet current densities flowing into and out of the ionosphere have been calculated separately for every local time hour. Results are presented in Fig. 2. FAC intensities are

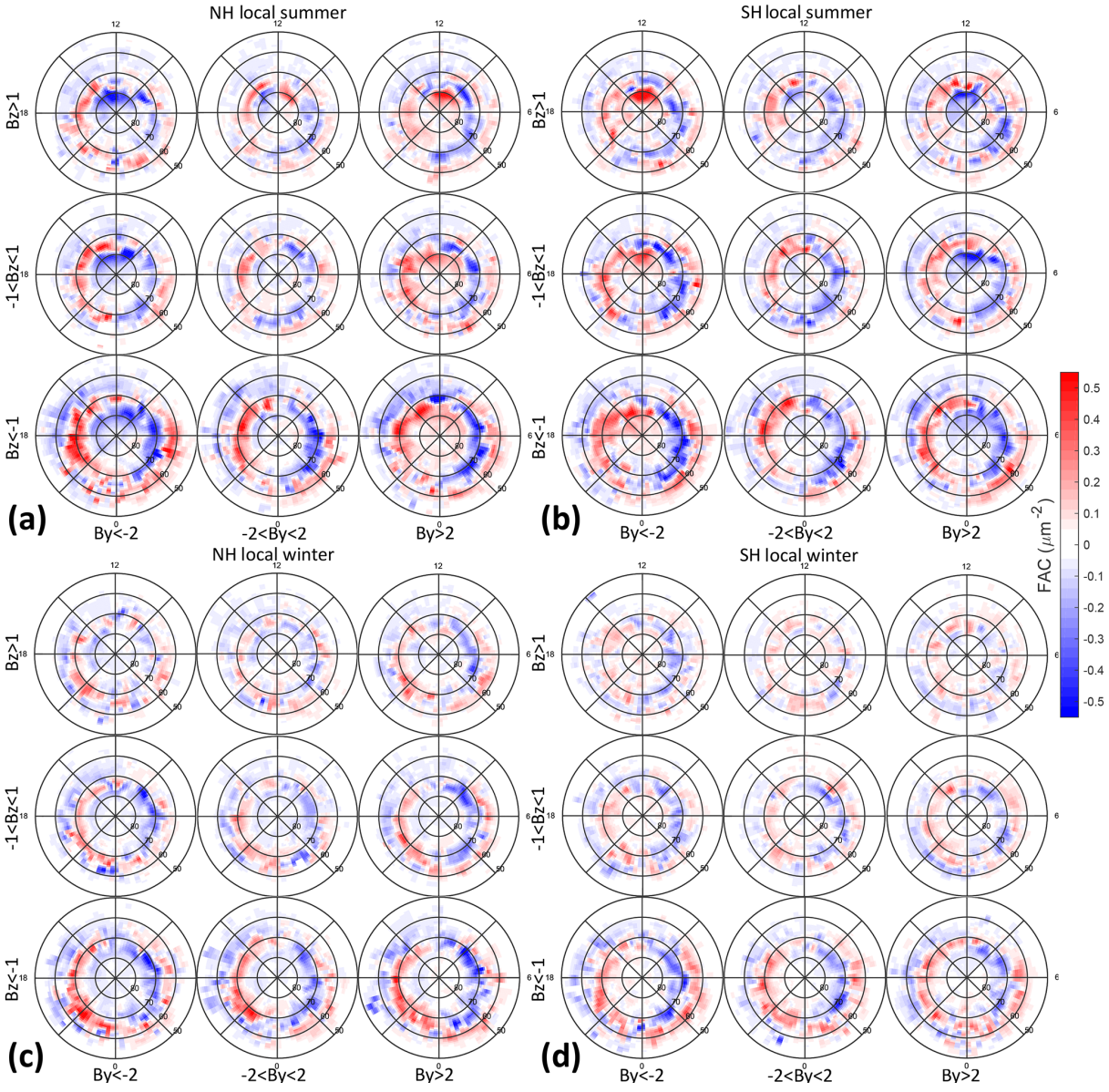

Figure 3. Maps of average FAC distribution in the Northern Hemisphere **(a, c)** and Southern Hemisphere **(b, d)** for local summer **(a, b)** and local winter **(c, d)**. The FAC distribution is shown in the frame of magnetic latitude (MLAT) versus magnetic local time (MLT) for $B_z > 1$, $-1 < B_z < 1$ and $B_z < -1$ conditions in rows from top to bottom in each panel. IMF B_y ranges change from $B_y < -2$, $-2 < B_y < 2$ to $B_y > 2$ from left to right columns. The blue (red) contours indicate downward (upward) currents.

clearly larger on the dayside during local summer (red lines) than local winter (blue lines). On the nightside the curves converge (in particular in the Northern Hemisphere); i.e., the seasonal dependence is much smaller. We regard the differences in FAC intensity primarily to changes in conductivity. On the dayside the ionospheric conductivity is mainly determined by the solar illumination. Therefore a strong seasonal dependence results. On the midnight side the auroral electron precipitation plays a more important role for the conductivity, making it less dependent on seasonal variations of solar insulation.

In the next step, we present the FAC distribution for different IMF orientations. The values are sorted into nine groups based on IMF B_y and B_z intensities in units of nT ($B_y < -2$, $-2 < B_y < 2$ and $B_y > 2$; $B_z < -1$, $-1 < B_z < 1$ and $B_z > 1$). Figure 3 shows the FAC distribution of bin averages in magnetic latitude versus local time frames in the Northern and Southern hemispheres separately. As before, the blue (red) contours represent the downward (upward) currents. Here we find even clearer differences between local summer (Fig. 3a and b) and local winter (Fig. 3c and d), with larger FAC den-

sity in local summer. This seasonal difference is obvious for all IMF directions.

Let us shortly introduce the IMF effects on the FAC patterns, as seen in Fig. 3. First the IMF B_z effect: it is obvious that the FACs are stronger under southward IMF conditions (bottom rows) in all of the panels. A southward IMF has been frequently reported to enhance the magnetosphere–ionosphere coupling due to magnetic reconnection (e.g., Iijima and Potemra, 1982). For northward IMF (top rows) we can observe NBZ currents in the summer hemisphere (Fig. 3a and b). The direction of these FACs, located mainly in the polar cap, depends strongly on the polarity of IMF B_y. For positive IMF B_y (right columns) FACs flow out of the polar cap in the Northern Hemisphere and into it in the Southern Hemisphere. Conversely, for negative IMF B_y (left columns) FACs flow out of the southern and into the northern polar cap. For small IMF B_y values (middle columns), an anti-parallel pair of FACs (upward before noon, downward after noon) appears in the polar caps of both hemispheres. All these characteristics of polar cap currents (also termed R0 FACs) have previously been reported (e.g., Stauning, 2002; Vennerstrøm et al., 2002; Wang et al., 2008b). These authors suggest that the absence of NBZ currents during local winter is due to the low conductivity in the polar cap. The sign of IMF B_y does not modify significantly the intensity of R2 currents. Changes in the R1 FACs in response to the IMF B_y polarity occur primarily around the noon sector. Here the dawn side R1 stretches past noon for positive IMF B_y and the dusk side R1 extends past noon for negative B_y in the Northern Hemisphere. The ionospheric FAC patterns in the Southern Hemisphere are mirror images of the Northern Hemisphere for all IMF B_y dependences. At local winter all the IMF B_y effects are almost negligible at this resolution.

Overall, our Swarm FAC patterns are consistent with previous results which are based on different data sets (e.g., Weimer, 2001; Christiansen et al., 2002; Papitashvili et al., 2002; Wang et al., 2005, 2008b; Anderson et al., 2008; Green et al., 2009; He et al., 2012). The main purpose of the presented FAC patterns is to provide the framework for interpreting the auroral Hall currents derived at the same time.

4 Distribution of auroral Hall currents

4.1 Estimating Hall currents from Swarm total field data

For the estimation of ionospheric Hall currents from satellite magnetic field measurements we use the line current approximation introduced by Olsen (1996). It interprets the variations of the total magnetic field component because this is practically unaffected by the strong FAC signals. This method was adopted for calculating Hall currents from Ørsted and CHAMP satellite data (Moretto et al., 2002; Ritter et al., 2004; Wang et al., 2008a). The Hall currents in the polar regions are approximated by a series of line currents at the height of 110 km and with a separation of 1° in latitude. The magnetic field at orbital altitude caused by an eastward-directed line current can be written as

$$b_x = -\frac{\mu_0 I}{2\pi}\frac{h}{x^2+h^2}, \qquad b_z = -\frac{\mu_0 I}{2\pi}\frac{x}{x^2+h^2}, \tag{4}$$

where b_x and b_z are the northward and downward components of the generated magnetic field, respectively. I is the current strength, h denotes the height above the current, and x is the northward displacement of the measurement point, with respect to the current location. The magnetic signature of the current in the total magnetic field can be represented as

$$\Delta F = |\mathbf{B}+\mathbf{b}| - |\mathbf{B}|, \tag{5}$$

where $\mathbf{B}$ is the unperturbed ambient magnetic field. The total field deflection ΔF is the signal we are interpreting here. Equation (5) can be replaced by the normalized dot product between $\mathbf{B}$ and $\mathbf{b}$ because $\mathbf{b}$ is much smaller than $\mathbf{B}$.

$$\Delta F = \frac{\mathbf{B}\cdot\mathbf{b}}{|\mathbf{B}|} \tag{6}$$

Equation (6) can be expanded for all the satellite positions in the form

$$\Delta F(j) = \frac{1}{|B|}\sum_i \left[p_x(i,j)\,B_X + p_z(i,j)\,B_Z\right] I(i), \tag{7}$$

where $p_x(i,j) = -\frac{\mu_0}{2\pi}\frac{h(i,j)}{x^2(i,j)+h^2(i,j)}$, $p_z(i,j) = -\frac{\mu_0}{2\pi}\frac{x(i,j)}{x^2(i,j)+h^2(i,j)}$. The index i numbers the line currents and j stands for the measurement points along a polar pass. Here the ambient fields B_X and $B_{Z,}$ are the northward and downward components in north, east, center (NEC) coordinates as derived from the CHAOS-6 model. With this equation we obtain a linear relation between the total field deflection and the various line current intensities $I(i)$. The observed total field residuals are inverted using a least-squares fitting approach to get the strength of each of the 100 line currents. For solving the inverse problem, a regularized least-squares approach is applied:

$$I = \left(G^T\mathbf{A}\mathbf{G}\right)^{-1} G\Delta F, \tag{8}$$

where $\mathbf{A}$ is a weighting matrix, which avoids oscillating results between neighboring line currents, $\mathbf{G}$ is the design matrix made up of known quantities such as positions and model magnetic fields. As a boundary condition for the line current inversion we assume vanishing current densities for latitudes below 50° MLAT. This removes false current estimates over the high-latitude orbit arc that may be caused by uncorrected ring current signals. The uncertainty of this Hall current estimate approach has been quantified by Ritter et al. (2004)

to 40 mA m^{-1} for a single profile, based on comparisons between results from ground-based and satellite data. More details about our Hall current density calculations can be found in Ritter et al. (2004). The distribution of Hall current sample numbers from Satellite A in each of the equal-area bins is shown in the Supplement (see Fig. S2). Thanks to the many orbits no bins contains less than 10 000 entries.

In this study the zonal component (east–west direction) of the Hall currents is estimated. Eastward (westward) directed currents have positive (negative) amplitudes. The zonal component is chosen because it gives the largest magnetic signal for a polar-orbiting satellite. Currents flowing in meridional direction (along the orbit) cannot be determined by this technique. As a consequence the current densities obtained in the polar cap may partly fall short with respect to the total sunward flow. This is an inherent limitation of our cross-track current estimate.

4.2 Dependence of Hall currents on season and IMF

By inverting the total field deflections, latitude profiles of Hall sheet current density can be obtained from each Swarm polar pass. For studying the characteristics of Hall currents, Fig. 4 shows the Hall current distribution during local summer and winter seasons under different IMF conditions, in the same format as for FACs in Fig. 3. Here again we use the defined seasons for June and December solstices, as given in Sect. 3.2. The eastward (westward) Hall current components derived from Swarm A are presented in red (blue) color. The Hall sheet current density is reflected by the color depth defined by the color bar. The numbers represent averages over the equal-area bins of 330 km × 350 km size distributed in the magnetic local time (MLT) versus magnetic latitude (MLAT) frame. Bins are placed in rings of magnetic latitude with a width of 3° MLAT, as described above (Sect. 3.2).

From Fig. 4 we can see that the average Hall currents show a rather distinct change in flow direction above and below 70° MLAT. Therefore we interpret the observations separately from these two latitude ranges. In the following we label them "polar cap" (PC: MLAT > 70°), and "auroral zone" (AZ: 60° ≤ MLAT ≤ 70°). Polar cap Hall currents are found to flow predominantly westward on the dawn side and eastward on the dusk side, meaning they are directed sunward on both sides (e.g., Ahn et al., 1999). In the auroral zone the auroral electrojets are located flowing anti-sunward both on the dawn and dusk sides, the inverse of polar cap Hall currents.

For the interpretation of our results we consider four separate local time sectors and label them: "noon sector" (10:00–14:00 MLT), "midnight sector" (22:00–02:00 MLT), "dawn sector" (02:00–10:00 MLT) and "dusk sector" (14:00–22:00 MLT). From each of the nine subplots in Fig. 4a–d we get a mean value of Hall current density from all the different sectors. Values are listed in Table 1a–d. The largest current densities are observed within the latitude range 60–70° MLAT, which can be related to the auroral electrojets. For representing their intensities, we take the mean value of all current densities from the bins, within the previously defined dawn and dusk sectors. As expected, the electrojet intensity is dependent on the solar wind input. This is represented by the merging electric field as defined in Eq. (1). Figure 5 shows the mean auroral current densities from the nine classes of IMF orientations plotted versus merging electric field, E_m, separately for the two solstices and two hemispheres. The different IMF orientations implicitly create a sufficiently large range of E_m variation. Excellent linear relations result in all cases. There is no sign of saturation observed for high solar wind input. Similar results have been reported by Zhou and Lühr (2017) for cross-polar cap ionospheric net currents. From Fig. 5 we cannot deduce any systematic dependence of the auroral electrojet intensities on IMF B_y orientation. As expected, current densities are generally higher in local summer (Fig. 5a and c) than in winter (Fig. 5b and d). This holds in particular for the eastward electrojet. Current values are somewhat larger in the Northern Hemisphere than in the Southern Hemisphere. The ratio between the slopes in the Northern and Southern hemispheres is approximately 1.6 for local summer, while it decreases to 1.0 in local winter. This holds in general for both the eastward and westward electrojets. Interestingly, current densities do not approach zero when E_m vanishes (due northward IMF). Some magnetospheric convection seems to remain even for that configuration. This is a known phenomenon, and the weak convection is thought to be driven by viscous interaction of the solar wind with the magnetosphere (see, e.g., Cowley, 1982; Tsurutani and Gonzalez, 1995).

4.2.1 Dependence on IMF orientation

For the IMF dependence one can see that the density of ionospheric Hall currents increases from top to bottom in all the rows of Fig. 4, and the maximum Hall currents occur when the IMF B_z component is southward. The equatorward boundary of the Hall currents moves towards lower latitude as the IMF B_z component changes from northward to southward. This can be attributed to the expanding polar cap due additional magnetic flux caused by dayside reconnection, as theorized by Siscoe and Huang (1985) and Cowley and Lockwood (1992), and seen also in the AMPERE-derived field-aligned current ovals by Clausen et al. (2012) and Coxon et al. (2014). As expected, the J_{Hall} values increase with E_m (see Table 1, from upper to lower rows), confirming that a southward IMF $B_z$component generally leads to stronger Hall currents in the ionosphere. The dependence on IMF B_y seems to be more interesting. Current densities from all six sectors are presented in Table 1 (the electrojets on dawn/dusk sides are not listed) and show clear variations with IMF B_y. Starting with the Northern Hemisphere and local summer, westward currents (blue color) dominate in Fig. 4a in the polar cap for negative IMF B_y. Conversely, for positive IMF

Table 1. (a) Northern Hemisphere summer average Hall current density for different IMF directions as in Fig. 3a. The results are sorted into two latitude ranges: polar cap (PC, MLAT > 70°) and auroral zone (AZ, 60° ≤ MLAT ≤ 70°) regions. The data are sorted into four MLT sectors (dawn: 02:00–10:00 MLT; noon: 10:00–14:00 MLT; dusk: 14:00–22:00 MLT; midnight: 22:00–02:00 MLT). Averages of Hall current densities and related uncertainties are given in units of mA m^{-1}. The merging electric field, E_m, is given in units of mV m^{-1}. The positive (negative) values indicate eastward (westward) Hall currents. **(b)** Same format as Table 1a, but for Southern Hemisphere local summer conditions. **(c)** Same format as Table 1a, but for Northern Hemisphere winter conditions. **(d)** Same format as Table 1a, but for Southern Hemisphere winter conditions.

(a)

NH		MLT	$B_y < -2$		$-2 < B_y < 2$		$B_y > 2$	
Local summer			J_{Hall}	E_m	J_{Hall}	E_m	J_{Hall}	E_m
$B_z > 1$	PC	10:00–14:00	-20.6 ± 52.5	0.6	18.9 ± 26.8	0.1	53.9 ± 46.7	0.5
		22:00–02:00	1.7 ± 13.5	0.5	22.4 ± 12.5	0.1	56.9 ± 12.4	0.4
	AZ	10:00–14:00	17.2 ± 10.9	0.6	16 ± 8.3	0.1	12 ± 9.8	0.5
		22:00–02:00	-13.6 ± 17.5	0.5	-11.5 ± 12.1	0.1	-12.8 ± 20.7	0.5
	PC	02:00–10:00	-10.5 ± 21.6	0.5	17.6 ± 18.9	0.1	53.1 ± 31.4	0.5
		14:00–22:00	-21.6 ± 36.3	0.5	9.9 ± 23.2	0.1	38.6 ± 20.1	0.5
$-1 < B_z < 1$	PC	10:00–14:00	-10.7 ± 55.6	1.0	27.8 ± 29.2	0.5	63.4 ± 53.2	1.1
		22:00–02:00	11.2 ± 17.1	1.0	32.1 ± 14	0.5	60.4 ± 15.4	1.0
	AZ	10:00–14:00	25.6 ± 13.9	1.1	17.8 ± 10.3	0.5	15.3 ± 8.8	1.1
		22:00–02:00	-25.7 ± 22.9	1.0	-18.5 ± 20.1	0.5	-23.4 ± 27.3	1.0
	PC	02:00–10:00	-6.9 ± 30.3	1.0	19.3 ± 23	0.5	55.6 ± 38.2	1.1
		14:00–22:00	-25.2 ± 39.9	1.0	18 ± 28.8	0.5	43.6 ± 31.4	1.1
$B_z < -1$	PC	10:00–14:00	-44.3 ± 71.5	2.4	27.4 ± 42.3	2.2	83.8 ± 70.3	2.8
		22:00–02:00	35.6 ± 25.2	2.4	57.7 ± 18.5	2.1	91.6 ± 25.6	2.4
	AZ	10:00–14:00	29.1 ± 20.8	2.4	27.7 ± 20.2	2.1	20.8 ± 28.8	2.9
		22:00–02:00	-60.9 ± 30.5	2.5	-45.6 ± 33.6	2.1	-60.2 ± 41.2	2.6
	PC	02:00–10:00	19.1 ± 53.7	2.3	42.2 ± 38.2	2.1	107 ± 39.2	2.4
		14:00–22:00	-50.4 ± 36.8	2.4	-0.1 ± 31.4	2.1	31.3 ± 40.4	2.5

(b)

SH		MLT	$B_y < -2$		$-2 < B_y < 2$		$B_y > 2$	
Local summer			J_{Hall}	E_m	J_{Hall}	E_m	J_{Hall}	E_m
$B_z > 1$	PC	10:00–14:00	25.2 ± 30.4	0.6	-4.3 ± 19.6	0.1	-37 ± 53.5	0.5
		22:00–02:00	51.2 ± 17.5	0.6	24.3 ± 18	0.1	2.8 ± 17.3	0.5
	AZ	10:00–14:00	4.3 ± 6.7	0.6	6.6 ± 5.8	0.1	12.5 ± 11.2	0.6
		22:00–02:00	-15.4 ± 23.2	0.6	-14.5 ± 13.6	0.1	-15.2 ± 17.1	0.5
	PC	02:00–10:00	44.7 ± 26.5	0.6	11.8 ± 17.4	0.1	-15.6 ± 18.8	0.5
		14:00–22:00	8.8 ± 19.8	0.5	-8.5 ± 18.2	0.1	-31.7 ± 26	0.5
$-1 < B_z < 1$	PC	10:00–14:00	27.1 ± 35.2	1.2	-5.8 ± 21.3	0.6	-35 ± 49.7	1.2
		22:00–02:00	60.6 ± 24.3	1.3	25.9 ± 17.1	0.6	1.7 ± 14.7	1.1
	AZ	10:00–14:00	5.3 ± 6.8	1.2	16.9 ± 16.9	0.6	13.4 ± 11.2	1.2
		22:00–02:00	-35.7 ± 31.4	1.2	-27 ± 28.8	0.6	-23.5 ± 22.4	1.1
	PC	02:00–10:00	54.5 ± 29.6	1.3	15.4 ± 21.5	0.6	-18.4 ± 33.4	1.2
		14:00–22:00	16.8 ± 24.5	1.2	-7.4 ± 22.7	0.6	-28.2 ± 26.8	1.2

Table 1. Continued.

(b)

SH		MLT	$B_y < -2$		$-2 < B_y < 2$		$B_y > 2$	
Local summer			J_{Hall}	E_{m}	J_{Hall}	E_{m}	J_{Hall}	E_{m}
$B_z < -1$	PC	10:00–14:00	10 ± 45.3	2.9	-28.2 ± 32	2.5	-64.2 ± 48.6	2.6
		22:00–02:00	85.7 ± 28.6	2.9	53.8 ± 19.8	2.5	22.6 ± 25.7	2.6
	AZ	10:00–14:00	7.5 ± 21.8	2.8	13.7 ± 18.1	2.4	22.6 ± 21.1	2.5
		22:00–02:00	-71 ± 52.7	2.9	-50.2 ± 38.9	2.4	-62 ± 38.3	2.5
	PC	02:00–10:00	69.5 ± 36.2	2.9	35.4 ± 31.9	2.4	6.9 ± 49.5	2.6
		14:00–22:00	-18.3 ± 30.9	2.9	-36.7 ± 30.7	2.5	-45 ± 28	2.6

(c)

NH		MLT	$B_y < -2$		$-2 < B_y < 2$		$B_y > 2$	
Local winter			J_{Hall}	E_{m}	J_{Hall}	E_{m}	J_{Hall}	E_{m}
$B_z > 1$	PC	10:00–14:00	-10.1 ± 19.1	0.5	0.9 ± 14.2	0.1	5.9 ± 12.2	0.5
		22:00–02:00	11.2 ± 13.2	0.5	14.6 ± 13	0.1	27.8 ± 15.8	0.5
	AZ	10:00–14:00	9.7 ± 6.1	0.5	10.8 ± 6.5	0.1	10.4 ± 6.3	0.5
		22:00–02:00	-14.7 ± 18.1	0.5	-22.9 ± 19.2	0.1	-24.8 ± 21	0.5
	PC	02:00–10:00	0.3 ± 16.7	0.6	5.2 ± 14.1	0.1	3.5 ± 22	0.5
		14:00–22:00	-15.9 ± 14	0.6	-7.6 ± 12	0.1	-4.8 ± 15.1	0.6
$-1 < B_z < 1$	PC	10:00–14:00	-13.6 ± 24.1	1.2	-0.3 ± 17.3	0.6	4.8 ± 18	1.2
		22:00–02:00	17.6 ± 16.3	1.2	12.4 ± 22.7	0.6	35.5 ± 23	1.2
	AZ	10:00–14:00	15.8 ± 6.5	1.2	13.5 ± 8	0.6	13.1 ± 6.8	1.1
		22:00–02:00	-30 ± 29.1	1.1	-31.4 ± 21.1	0.6	-51.7 ± 30.4	1.2
	PC	02:00–10:00	3.2 ± 25.1	1.3	8.9 ± 19	0.6	3.2 ± 26.5	1.2
		14:00–22:00	-18.7 ± 21	1.3	-8.9 ± 16.7	0.6	-5.9 ± 18	1.2
$B_z < -1$	PC	10:00–14:00	-38.4 ± 28.7	2.9	-20.3 ± 21	2.6	-15.3 ± 22.5	2.6
		22:00–02:00	37.3 ± 29.7	2.8	41.9 ± 31.8	2.4	57.8 ± 29.6	2.5
	AZ	10:00–14:00	18.1 ± 15	2.8	20.7 ± 12	2.5	21.9 ± 14	2.5
		22:00–02:00	-68.1 ± 42.4	2.8	-72 ± 44.6	2.2	-94.6 ± 46.7	2.5
	PC	02:00–10:00	10.7 ± 40.6	2.9	22.5 ± 34.8	2.6	22.2 ± 37.4	2.6
		14:00–22:00	-41.8 ± 21	2.9	-25.1 ± 22.2	2.5	-22.3 ± 24.5	2.5

(d)

SH		MLT	$B_y < -2$		$-2 < B_y < 2$		$B_y > 2$	
Local winter			J_{Hall}	E_{m}	J_{Hall}	E_{m}	J_{Hall}	E_{m}
$B_z > 1$	PC	10:00–14:00	-2.5 ± 9.5	0.5	2 ± 6.3	0.1	-6.1 ± 11.3	0.5
		22:00–02:00	23.4 ± 14.8	0.5	7.3 ± 9.4	0.1	6.7 ± 10.1	0.5
	AZ	10:00–14:00	4.7 ± 5.4	0.5	6.8 ± 3.1	0.1	6.9 ± 2.8	0.4
		22:00–02:00	-33.9 ± 22.1	0.5	-8.2 ± 14.1	0.1	-4.9 ± 11	0.5
	PC	02:00–10:00	2.2 ± 15.5	0.5	2.5 ± 8.5	0.1	2 ± 9.4	0.5
		14:00–22:00	-4.7 ± 7.9	0.5	1.5 ± 5	0.1	-5.3 ± 8.3	0.5

Table 1. Continued.

(d)								
SH		MLT	$B_y < -2$		$-2 < B_y < 2$		$B_y > 2$	
Local winter			J_{Hall}	E_{m}	J_{Hall}	E_{m}	J_{Hall}	E_{m}
$-1 < B_z < 1$	PC	10:00–14:00	-0.8 ± 14	1.1	-1 ± 10.1	0.5	-7 ± 13.3	1.1
		22:00–02:00	21.1 ± 19.4	1.0	9.8 ± 16.9	0.6	7.7 ± 16.6	1.1
	AZ	10:00–14:00	8.4 ± 5.4	1.0	8 ± 3.6	0.5	8.5 ± 5	1.1
		22:00–02:00	-43.9 ± 30.9	1.1	-19.4 ± 15.6	0.6	-18 ± 15.8	1.1
	PC	02:00–10:00	6.5 ± 16.3	1.1	6.4 ± 13.1	0.6	4 ± 15.4	1.1
		14:00–22:00	-7.5 ± 13.5	1.0	-2.9 ± 9.7	0.5	-11.5 ± 10	1.1
$B_z < -1$	PC	10:00–14:00	-8.7 ± 24.9	2.3	-7.3 ± 18.4	2.1	-23.1 ± 20.4	2.5
		22:00–02:00	61.1 ± 32.1	2.4	40.9 ± 31	2.2	34 ± 28.7	2.6
	AZ	10:00–14:00	9.2 ± 16.2	2.3	10.5 ± 9.6	2.1	8.1 ± 11.9	2.5
		22:00–02:00	-69.6 ± 32.4	2.5	-55.9 ± 31.7	2.2	-66.9 ± 43.1	2.9
	PC	02:00–10:00	26.6 ± 30.4	2.3	18.6 ± 27.5	2.2	17.4 ± 32.4	2.6
		14:00–22:00	-19.8 ± 17.3	2.4	-13 ± 15.3	2.1	-33.1 ± 17.7	2.5

B_y, red color dominates (eastward currents) in the polar cap. This can be related to two processes. In the noon sector we have downward FACs in the polar cap (R0), and adjacent to it upward R1 FACs for negative IMF B_y (see Fig. 3). Between these FAC sheets a westward Hall current is observed. Opposite current directions are observed for positive IMF B_y field. This has earlier been termed the DPY current system (e.g., Wilhjelm et al., 1978). Quantitative values for the intensity of the DPY system can be found in Table 1 (PC, 10:00–14:00). The other process is the electrojet return current over the polar cap. In the case of a positive IMF B_y the plasma convection cell is large on the dusk side focusing the sunward return current on the dawn side (eastward current). Conversely, for negative IMF B_y a strong westward (sunward) return current is focused on the dusk side. An equally distributed return current density is found for small IMF B_y. The midnight substorm electrojet, presented in Fig. 6, shows little dependence on IMF B_y or on season. As expected, mirror images of IMF B_y-dependent Hall currents appear in the Southern Hemisphere (see Fig. 4b).

4.2.2 Seasonal dependence

The seasonal dependence is obvious from a comparison of the colors in the top (local summer) and bottom (local winter) panels of Fig. 4. The ionospheric Hall currents are generally stronger in local summer than in local winter. It is more appropriate to compare the Hall current densities in different regions and MLT sectors separately. Here we start with the noon polar cap sector. In this region particularly large differences between the seasons are observed. The Hall current densities are smaller by factors of 5 to 10 in both hemispheres during winter conditions. Similarly for the sunward return current, the average ratio of cross-polar cap Hall current density between local summer and local winter varies between 2 and 5 in the hemispheres according to Table 1 (PC, 02:00–10:00 and 14:00–22:00). Even more interestingly, the IMF B_y dependence of all polar cap currents seems to vanish. More details on this will be presented in Sect. 5.4.

The seasonal ratio is clearly smaller for the electrojets, as can be seen in Fig. 5. The smaller difference of the westward electrojet compared to the eastward electrojet between summer and winter conditions is probably due to a larger contribution of precipitating auroral particles in the dawn sector to the overall conductivity, Newell et al. (2010) reported that the diffuse precipitation, which is important for conductivity enhancement, dominates the dawn sector (see their Fig. 2). This effect is probably the cause for the reduced seasonal dependence in that sector. An even smaller seasonal dependence is observed for the substorm-related electrojet around midnight. In Fig. 6 we find a small dominance of current density during December season in both hemispheres.

Concerning the uncertainty of current densities listed in Table 1, the standard deviation associated with the mean values is rather large due to the large variability of observed current density. We therefore prefer the uncertainty of mean value in this study, which is the standard deviation divided by the square root of the number of independent samples (e.g., number of passes contributing to a bin). This uncertainty is added to the mean values in Table 1.

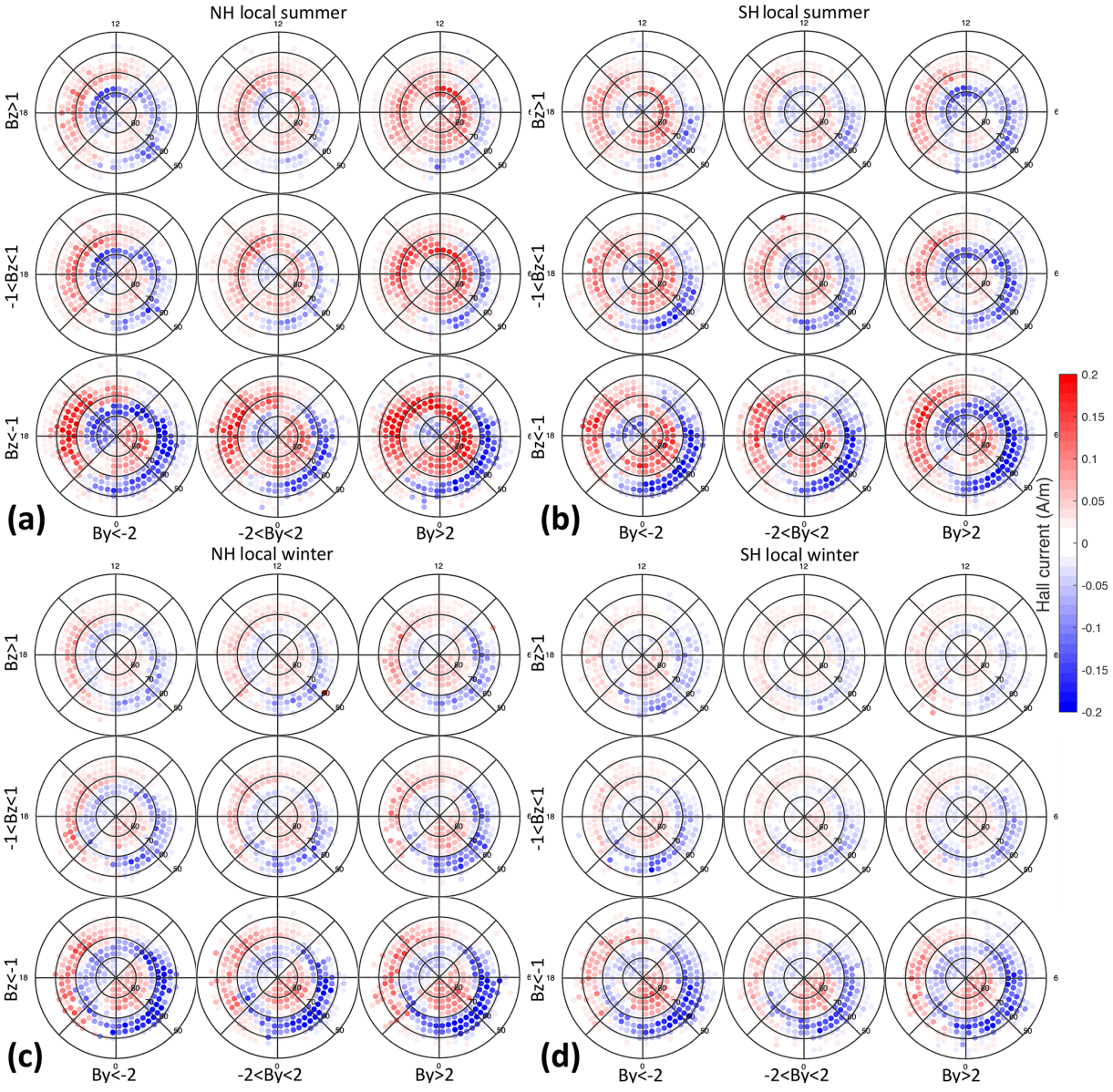

Figure 4. Maps of the average Hall current distribution in the same format as Fig. 3. The red (blue) dots represent eastward (westward) currents. Here the currents mainly flow anti-sunward along the auroral oval and sunward in the polar cap.

5 Discussion

After having presented the general features of the auroral Hall currents we will discuss in this section the observed characteristics of the different components one by one.

5.1 Assessment of Hall current estimates

In general, ionospheric Hall currents are assumed to flow in closed circuits at high latitude. However, in the case of conductivity gradients, part of the Hall current is diverted by FACs into space. In a recent study (Zhou and Lühr, 2017) quantified the amount of Hall current that is not closed in the ionosphere. Here we address whether we have recovered the full Hall current or only the source-free part of it. In order to validate Hall current estimations, we have tried to determine with our approach the net current in anti-sunward direction (which is not closed in the ionosphere) as was done by Zhou and Lühr (2017) but using a different approach. For calculating the expected anti-sunward current the derived current densities are summed up along each Swarm high-latitude arc on dawn–dusk (05:00–07:00 or 17:00–19:00 MLT) orbits. The summed current density is multiplied by the distance between data points (7.6 km) in order to get the net current. Figure 7 shows the distribution of obtained anti-sunward net Hall current in units of kA for the different months of a

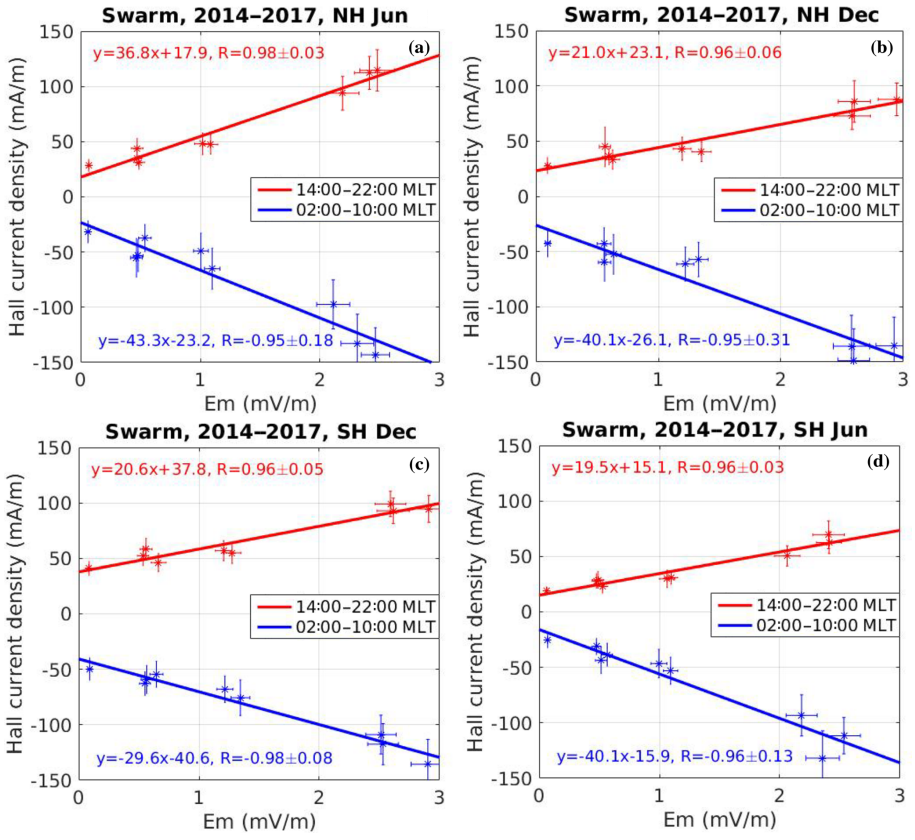

Figure 5. The relationship between mean Hall current density and E_m for the dawn and dusk side auroral electrojets. The error bars indicate the uncertainty of mean values both for E_m and Hall current density.

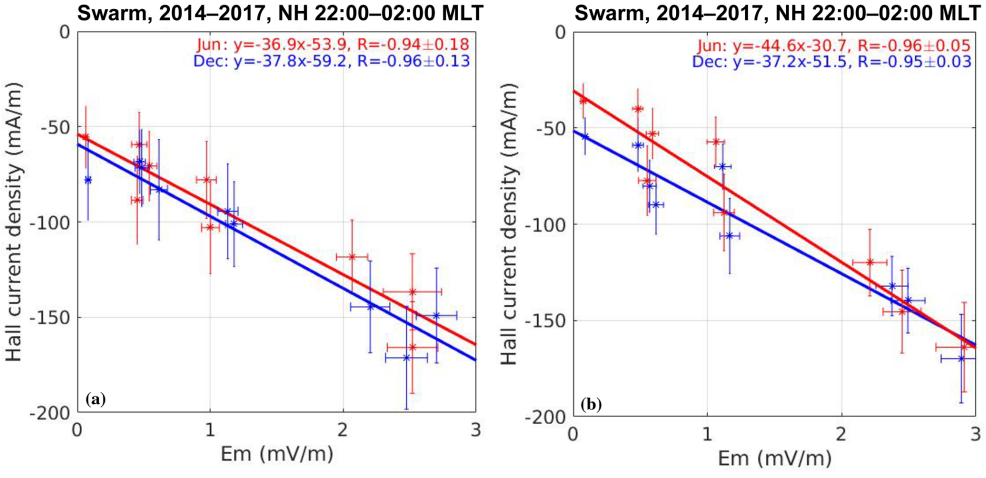

Figure 6. The relationship between E_m and substorm electrojet in the midnight sector. The red (blue) line is used for June (December) solstice. Panels **(a)** and **(b)** represent the Northern and Southern hemispheres, respectively.

year for the Northern and Southern hemispheres separately. In the Northern Hemisphere we find values varying between −30 kA and +30 kA with a clear minimum at July. In the Southern Hemisphere similar values for net currents are obtained, but here the minimum appears around January. Negative values during local summers represent unrealistic sunward net currents.

For the interpretation of the currents in Fig. 7, we compare them with the results of the dedicated study on auroral net currents by Zhou and Lühr (2017). In their Fig. 7

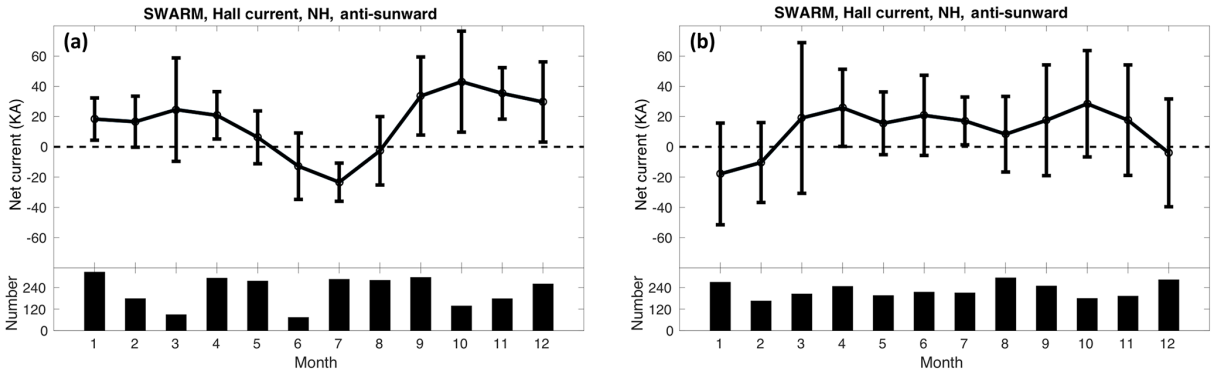

Figure 7. Annual variation of net currents flowing from the day to night side. In the two hemispheres opposite annual variations are observed. The error bar indicates the uncertainty of the values. In the bottom panels the number of contributing orbits are shown.

they show the average annual variation of anti-sunward net currents for the two hemispheres. As expected, these currents are systematically anti-sunward and strongest during local winter when the polar cap conductivity is reduced, and they show a minimum in local summer. By and large, the shapes of our curves in Fig. 7 are the same as in their Fig. 7. Also, the peak-to-peak annual variations reported by Zhou and Lühr (2017), NH: 50 kA and SH: 70 kA, are in agreement with our observations. A clear difference is the lack of an annual mean value of about 170 kA of anti-sunward current reported by Zhou and Lühr (2017). This lack of the anti-sunward bias is probably caused by our boundary condition forcing the current densities to approach zero for latitudes below 50° MLAT. Thus the actual electrojet currents are somewhat stronger (on average about 40 kA when split evenly between dawn and dusk sides) and the return current over the polar cap is correspondingly weaker than presented here. The missing part of electrojet current, ΔI_{EJ} (in kA), depending on the merging electric field, can be approximated by $\Delta I_{\mathrm{EJ}} = 50 E_{\mathrm{m}}$ according to the values given in Table 1 of Zhou and Lühr (2017). This lack of the mean part of the anti-sunward net current, however, does not change the dependences of Hall current density on environmental conditions.

5.2 Electrojets

As shown in Fig. 4, the auroral electrojets originate near the noon sector and flow anti-sunward along the dawn and dusk auroral zones. The amplitudes of the directly driven electrojets depend linearly on E_{m} (see Fig. 5). Magnetic ground signatures of the electrojets in the Northern Hemisphere are taken to construct the auroral activity index, AE, which is commonly used as a measure of energy input. The intensities of eastward and westward electrojets are comparable in the summer hemisphere due to the solar-driven conductivity. One interesting point is that the values in the Northern Hemisphere are larger than in the Southern Hemisphere during local summers (see Fig. 5a and c). A similar hemispheric asymmetry was reported by other studies. Coxon et al. (2016) found that total FAC magnitude differences, $J_{\mathrm{N}} - J_{\mathrm{S}}$, measured by AMPERE and averaged over one solar rotation were larger during the northern summer (3.1 MA) than the southern summer (−1.1 MA). They attributed the larger current magnitudes to a stronger reaction to dayside reconnection rate and higher ionospheric conductance in Northern Hemisphere during June solstice. From auroral net current results, Zhou and Lühr (2017) inferred a higher ionospheric conductivity by a factor of 1.5 in the Northern Hemisphere compared to the Southern Hemisphere during local summers. No such hemispheric differences were reported by them for winter seasons. On the other hand, the westward and the eastward electrojets are not balanced in the winter hemispheres. In fact the westward electrojet on the dawn side is stronger than the eastward electrojet on the dusk side in that season. Such an imbalance was also reported by Guo et al. (2014) for the Northern Hemisphere (see their Fig. 2). For winter they find a mean magnitude of the eastward electrojet of about 0.13 MA, while the westward electrojet reaches about 0.22 MA. The maximum eastward electrojet in winter is attributed by those authors to the northward convection electric field, which dominates over the Hall conductance. The authors further claim that the westward electrojet is occasionally fed by the closure of the substorm current wedge and enhanced in the midnight sector where substorms mainly occur. All these statements are consistent with our observations. In addition we think that the westward electrojet on the dawn side is also intensified during local winter due to a conductivity enhancement by precipitating particles (see also our arguments in Sect. 4.2.2).

In our observation no obvious dependence of the electrojet intensity on the sign of IMF B_y could be found. Although the overall morphology of auroral currents changes with IMF B_y orientation, as shown in Fig. 4, the mean intensities of the electrojet are hardly affected. One interesting result that can be inferred from our analysis: the AE index, derived from the auroral electrojet intensity in the Northern Hemisphere, can be regarded as a suitable indicator for global solar wind in-

put with just a little seasonal dependence, an underestimation around December solstice.

For completeness we address here a part of the Hall current at auroral/subauroral latitudes (equatorward of 70° MLAT) around the noon sector that has received little attention so far. In both hemispheres we find moderate current densities in this region (see Table 1a and c (AZ, 10:00–14:00) and Fig. S3). The current direction is generally eastward, regardless of IMF B_y orientation. Current densities reduce by a factor of 2 during local winter, which is consistent with the ratio of conductivity change between the seasons. When looking at the average FAC distribution in that sector (see Fig. 1) we find predominantly weak downward FACs at subauroral latitudes in both hemispheres. Poleward of these FACs the plasma is expected to flow westward, which is assumed to be part of the dusk convection cell. We regard the Hall currents observed around noon as caused by this subauroral plasma flow. In that sense the current can be considered as an extension of the eastward electrojet into the subauroral noon sector.

5.3 NBZ and DPY currents

In Sects. 3 and 4 we presented the patterns of FACs and Hall currents derived simultaneously from Swarm satellites. The dayside Hall currents correlate well with FACs in the polar cap. In particular during northward IMF significant FAC activity is observed poleward of the cusp, commonly termed R0 FACs (see Fig. 3). The direction of those currents depends on the sign of IMF B_y. We also observe Hall currents associated with this NBZ current system in the noon sector at high latitudes. All these FAC features during northward and dusk-ward IMF periods are consistent with the model results of Wang et al. (2008b).

For visualizing the IMF dependence of Hall currents in the polar cap we have plotted the zonal current directions separately for all four of our local time sectors in IMF B_y versus B_z frames. Figure 8 shows situations in the Northern Hemisphere during summer. In the noon sector (Fig. 8a) there appear westward currents in the case of negative IMF B_y and eastward ones for positive B_y. On average eastward currents dominate over the westward currents. We attribute this to the systematic skewing of the convection pattern toward pre-noon hours due to the corotation electric field. The skewing angle is larger for positive IMF B_y (e.g., Cowley, 2000). In that case part of the eastward electrojet on the dusk side is shifted into our symmetrical noon sector, making contributions to the mean value.

For positive IMF B_z the observed Hall currents are related to the NBZ system. Zonal currents in the high-latitude noon sector during negative IMF B_z are considered to be part of the DPY system (e.g., Friis-Christensen and Wilhjelm, 1975). Field lines, newly opened by magnetic reconnection on the dayside, are significantly curved in the presence of an IMF B_y component. The resulting magnetic tension causes azimuthal plasma drifts in the high-latitude ionosphere. Their directions depend on the IMF B_y sign. As a consequence, Hall currents flow in opposite direction when sufficient conductivity exists (e.g., Erlandson et al., 1988). Consistent with that notion we observe westward currents for negative IMF B_y and eastward for positive B_y. The dominance of eastward Hall current density also for the DPY system is again due to the skewing of the convection patterns, as explained above.

Some researchers (e.g., Belehaki and Rostoker, 1996) like to interpret these horizontal DPY currents as extensions of the electrojets connecting to the sunward return currents over the polar cap. Our observations in the Northern Hemisphere during local summer (Fig. 4a) seem to confirm the existence of such a connection. For negative IMF B_z and positive IMF B_y we find a dominant eastward Hall current circuit from the afternoon electrojet towards the dawn side return current over the polar cap and then the eastward DPY current that connects to the electrojet. For negative IMF B_y a corresponding westward Hall current loop dominates. Rather comparable current configurations can be found in the Southern Hemisphere noon sector around December solstice, but for opposite IMF B_y signs (see Fig. S1).

In the winter hemispheres we observe a quite different dependence on IMF B_y. The NBZ-related Hall currents are practically non-existent (see Fig. 9a). Instead of DPY currents, we observe for negative IMF B_z only westward currents in the winter hemispheres, independent of IMF B_y orientation. We assume these are connected to the westward electrojet on the dawn side. In the Southern Hemisphere appear similar currents in the polar cap noon sector around June solstice, and they have the same direction (see Fig. S1).

5.4 Sunward return currents

Based on our observations of the Hall current patterns we find sunward current flows over the polar cap. It has to be kept in mind that we present here only the east–west component of the current. Therefore values around the noon and midnight sectors may not reflect the full return current flow. During local summer, when the polar cap is continuously sunlit, the major part of electrojet currents closes across the polar cap. Inversely, in the winter hemisphere, a significant part of the electrojet currents is diverted into FACs, downward near noon and upward near the midnight sectors (e.g., Zhou and Lühr, 2017).

The return current does not flow homogeneously across the polar cap, as can be seen in Fig. 4a. In the Northern Hemisphere sunward current densities are much higher on the dawn side for positive IMF B_y. Conversely, more intense return currents appear on the dusk side for negative IMF B_y. An even more detailed picture emerges from Fig. 8c and d where the directions of Hall currents show dependences on IMF B_y and B_z. It is confirmed here that for positive IMF B_y most of the return current flows on the dawn side (red color). Similarly, the blue color on the dusk side (Fig. 8c)

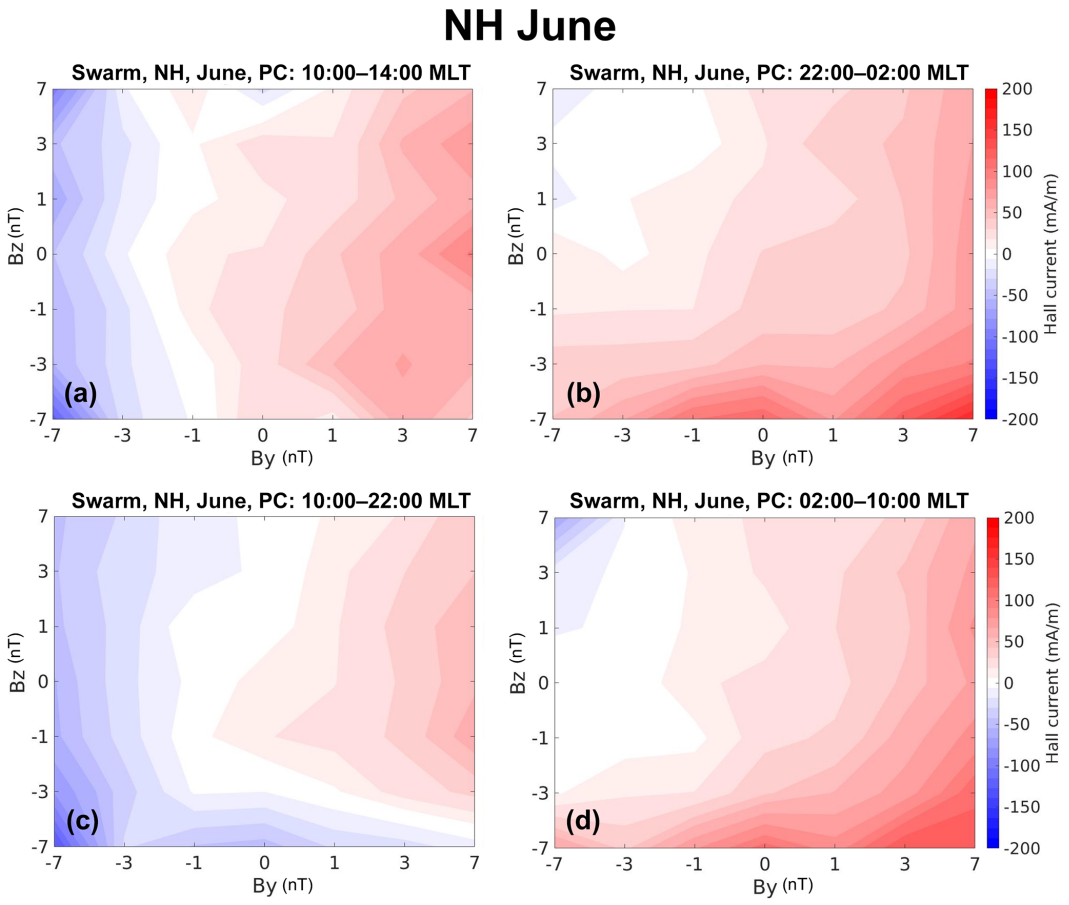

Figure 8. IMF dependence of polar cap Hall current flow direction in the Northern Hemisphere during June solstice (local summer). Eastward (westward) currents are shown in red (blue).

represents return currents for negative IMF B_y. However, on the dusk side we find also anti-sunward currents (red color) for positive IMF B_y and a corresponding patch of blue color (sunward current) in Fig. 8d.

This notion of Hall currents in the local summer can only be understood when considering the FAC distribution in the polar cap, in particular during northward IMF. As can be seen in Fig. 3a, there are primarily upward FACs at high latitudes in the case of positive IMF B_y, placing the region of large dusk-ward potential differences deep into the dawn sector. Similarly, the presence of downward FACs in the polar cap for negative IMF B_y pushes the location of largest electric fields and currents towards the dusk side. This allows anti-sunward currents to flow in the opposite time sector. In that sense our FACs and Hall current observations are highly consistent. For more southward IMF conditions the anti-sunward polar cap currents disappear. Corresponding characteristics but with opposite IMF B_y dependence can be found in the Southern Hemisphere (see Figs. S5 and S6).

During local winter season, the details in response to the IMF B_y dependence disappear also in the case of polar cap return currents, as can be seen in Fig. 9c and d. There are weak but exclusively sunward currents both on the dawn and dusk sides. The absence of IMF B_y dependence is also found in the Southern Hemisphere around June solstice.

For completeness, Fig. 9b shows the polar cap current on the nightside. Here eastward currents are clearly dominating. They become stronger for more negative IMF B_z and positive B_y. This notion, valid for summer and winter conditions and for both hemispheres, can be explained by the clockwise skewing of the convection patterns, which is more pronounced for negative IMF B_y.

The relations between FACs and Hall currents for the various IMF orientations, as derived from our observations for summer conditions, have been summarized in Fig. 10 by means of schematic drawings. Displayed is the situation for the Northern Hemisphere. Colored ellipses with dots and crosses represent regions of upward and downward FAC sheets, respectively. Region 2 FAC sheets have been omitted for clarity. The green dashed line marks the separatrix between the clockwise and counterclockwise convection cells, deduced from our ionospheric currents observations. Black arrows indicate the flow of Hall currents. Generally, the Hall current circulates around FAC regions in the polar region.

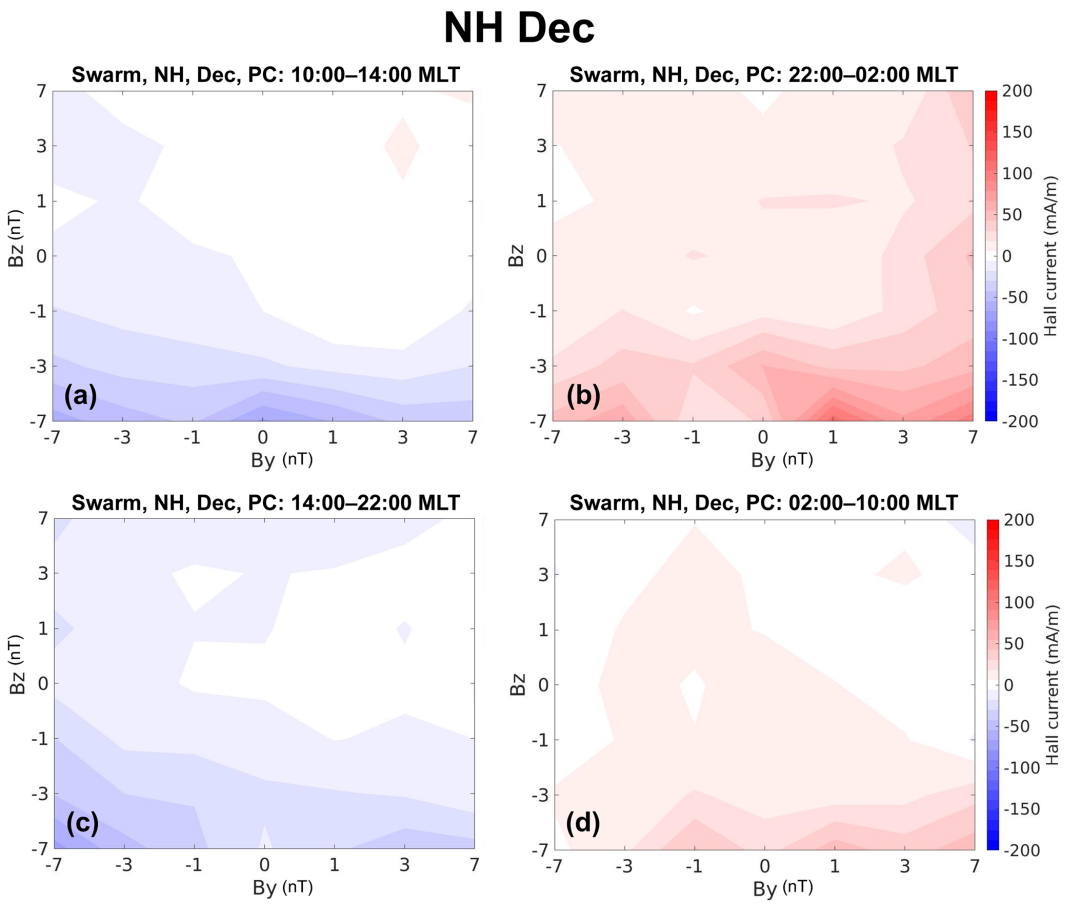

Figure 9. Same format as Fig. 8 but for December solstice (local winter).

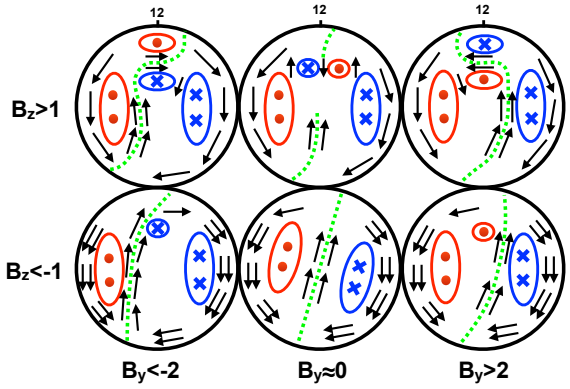

Figure 10. Schematic drawing of Hall current distributions for various IMF orientations. Colored ellipses with dots and crosses represent upward and downward FAC regions, respectively. Region 2 FACs have been omitted. The dotted green lines mark the separatrix between the two convection cells. Black arrows indicate the flow of Hall currents. The image represents the situation in the Northern Hemisphere for summer conditions.

For IMF $B_y > 0$ ($B_y < 0$) the upward (downward) R0 FAC at high latitudes together with the respective R1 current occupy a larger area on the dusk side (dawn side) than the downward (upward) R1 FAC sheet on the dawn side (dusk side). Correspondingly, the Hall return currents are more concentrated on the dawn side (dusk-ward) in the polar cap.

During times of extended northward IMF a pair of oppositely directed FACs appear in the high-latitude noon sector, commonly termed NBZ currents. Their orientation is closely controlled by the IMF B_y component, as described, e.g., by Vennerstrøm et al. (2002) and illustrated in Fig. 10. Our observations confirm this switch in Hall current direction for the two signs of IMF B_y. We see in Figs. 4a and 8a for IMF $B_y > 0$ ($B_y < 0$) eastward (westward) currents, as shown in Fig. 10. For small IMF B_y conditions a four-cell convection pattern is expected in connection with the NBZ system (see Huang et al., 2000). The anti-sunward meridional Hall currents expected in the noon sector, however, cannot be detected by our approach, but the related pair of oppositely directed FACs at high latitudes is visible in Fig. 3a and b.

5.5 Substorm electrojet

Finally, we have a look at the auroral Hall currents on the nightside. Here we find exclusively a dominance of westward currents. They can be related to the substorm electrojet. According to Fig. 6, the average current density is closely controlled by magnetic activity, in our case represented by the merging electric field, E_m. However, there appears to be no obvious dependence on IMF B_y. Our observations suggest a fairly linear dependence of current density on E_m. The derived slopes are larger than those obtained for the electrojets. They vary around $j \approx 40\,E_m$, where E_m is in units of $mV\,m^{-1}$ and j in $mA\,m^{-1}$ fairly independent of season and hemisphere. Interestingly, the current density does not reach zero for vanishingly E_m, which is also the case for the electrojets (see Fig. 5). When interpreting these average values, we have to keep in mind that substorms are discrete events. It would be more appropriate to synchronize the nighttime current measurements with the occurrence and phase of a substorm, as was done, e.g., by Ritter et al. (2010). Then the obtained FAC and Hall current measurements could be better related to the processes operating during substorms. Such an approach should be the topic of a follow-up study.

6 Summary

This study focuses on the seasonal and IMF dependence of FAC and Hall currents within the auroral ionosphere. The results are derived from 3 years of Swarm magnetic field measurements. It is the first study considering global distributions of FACs and Hall currents estimated simultaneously. The obtained results are consistent with previous studies of auroral zone current configuration, but here we provide a comprehensive picture of all these effects derived from a single and homogeneous data set. In addition quantitative values are listed for mean current densities and dependences on solar wind input and IMF orientation.

The FAC patterns are derived from the dual-spacecraft method, which provides more reliable results in particular at polar cap latitudes. Qualitatively, the obtained FAC distribution is consistent with previous results.

The primary aims of this study is determining the statistical proprieties of the auroral Hall currents. Our technique of Hall current estimation returns predominantly the source-free part of the Hall currents. This causes a certain underestimation of the electrojet intensity and an overestimation of the return currents over the polar cap. Approaches for first-order corrections are offered.

The auroral electrojets are an important part of the Hall current system. Their intensity is closely controlled by the solar wind input represented here by the merging electric field, calculated in a similar way as the Newell coupling function. The eastward electrojet on the dusk side shows a seasonal dependence reflecting the difference in ionospheric conductivity between local summer and winter solstices. Conversely, the westward electrojet does not change much over the seasons. Obviously precipitating electrons play an important role, besides solar insulation, in the conductivity on the dawn side. We could not identify any significant dependence of the electrojet intensities on the IMF B_y orientation.

The main part of the electrojet current is closed by sunward return currents flowing over the polar cap. The intensity of return currents is directly proportional to ionospheric conductivity, which is on average twice as strong during local summer as winter. The current flow is not homogenously distributed over the polar cap, but it is strongly dependent, in the summer hemisphere, on the IMF B_y orientation. For positive IMF B_y we find in the Northern Hemisphere a concentration of current density on the dawn side. Conversely, the highest current density appears on the dusk side in the case of negative IMF B_y. Opposite B_y dependences are observed in the Southern Hemisphere around December solstice.

In the noon sector the direction of Hall currents is also highly dependent on IMF B_y orientation. For positive IMF B_y, eastward Hall currents dominate in the Northern Hemisphere and westward currents for negative B_y. In the case of positive IMF B_z these Hall currents are part of the additional convection cells on the dayside, which are related to the NBZ system. It is practically absent during local winter in the dark hemisphere. For negative IMF B_z conditions, more intense Hall currents appear around noon. Also here eastward Hall currents dominate for positive IMF B_y and westward currents for negative B_y. In the past, they have been found to be linked to the DPY system. Comparable Hall current distributions appear in the Southern Hemisphere around December solstice but with opposite IMF B_y dependences.

Hall currents around the midnight sector are related to substorm activity. On average they are flowing westward independent of IMF B_y or B_z orientation. Their intensity is closely controlled by magnetic activity. They show little dependence on season when normalized to a fixed level of magnetic activity.

An important conclusion of this study is that IMF B_y-dependent variations of the FAC and Hall current configurations, which appear with opposite senses in the conjugate hemispheres, disappear during local winter seasons. This observation should be considered in empirical models of auroral current systems that are parameterized by IMF orientations.

This initial study shows the potentials of the Swarm mission for visualizing the general distribution of auroral currents. For a comprehensive climatology of the currents, at least 5 years of Swarm magnetic field observations would be needed. Such a time interval assures even data coverage of local times during all seasons.

Data availability. The calibrated 1 Hz Swarm magnetic field data (MAGx_LR) are available at ftp://swarm-diss.eo.esa.int (login re-

quired; access permission can be requested via https://earth.esa.int/Swarm). The CHAOS-6 model is available from www.spacecenter.dk/files/magnetic-models/CHAOS-6. For the solar wind input, the OMNI data are available at ftp://spdf.gsfc.nasa.gov/pub/data/omni/high_res_omni/.

The Supplement related to this article is available online at https://doi.org/10.5194/angeo-35-1249-2017-supplement.

Competing interests. The authors declare that they have no conflict of interest.

Acknowledgements. The European Space Agency (ESA) is acknowledged for providing the Swarm data and for financially supporting the work on developing the Swarm Level 2 Product "FAC". Hui Wang and Tao Huang acknowledge support from the National Nature Science Foundation of China (no. 41674153, 41521063, 41431073). The work of Tao Huang at GFZ Potsdam is supported by the China Scholarship Council (no. 201506270072).

The article processing charges for this open-access publication were covered by a Research Centre of the Helmholtz Association.

The topical editor, Steve Milan, thanks John Coxon, Ryan McGranaghan, and one anonymous referee for help in evaluating this paper.

References

Ahn, B.-H., Emery, B. A., Kroehl, H. W., and Kamide, Y.: Climatological characteristics of the auroral ionosphere in terms of electric field and ionospheric conductance, J. Geophys. Res.-Space, 104, 10031–10040, https://doi.org/10.1029/1999JA900043, 1999.

Anderson, B. J., Korth, H., Waters, C. L., Green, D. L., and Stauning, P.: Statistical Birkeland current distributions from magnetic field observations by the Iridium constellation, Ann. Geophys, 26, 671–687, https://doi.org/10.5194/angeo-26-671-2008, 2008.

Belehaki, A. and Rostoker, G.: Relationship between the dayside auroral electrojets and the DPY current, J. Geophys. Res.-Space, 101, 2397–2414, https://doi.org/10.1029/95JA02390, 1996.

Carter, J. A., Milan, S. E., Coxon, J. C., Walach, M.-T., and Anderson, B. J.: Average field-aligned current configuration parameterized by solar wind conditions, J. Geophys. Res.-Space, 121, JA021567, https://doi.org/10.1002/2015JA021567, 2016.

Christiansen, F., Papitashvili, V. O., and Neubert, T.: Seasonal variations of high-latitude field-aligned currents inferred from Ørsted and Magsat observations, J. Geophys. Res.-Space, 107, 13 pp., https://doi.org/10.1029/2001JA900104, 2002.

Clausen, L. B. N., Baker, J. B. H., Ruohoniemi, J. M., Milan, S. E., and Anderson, B. J.: Dynamics of the region 1 Birkeland current oval derived from the Active Magnetosphere and Planetary Electrodynamics Response Experiment (AMPERE), J. Geophys. Res.-Space, 117, A06233, https://doi.org/10.1029/2012JA017666, 2012.

Cowley, S. W. H.: The causes of convection in the Earth's magnetosphere: A review of developments during the IMS, Rev. Geophys. Space Ge., 20, 531–565, https://doi.org/10.1029/RG020i003p00531, 1982.

Cowley, S. W. H.: Magnetosphere-Ionosphere Interactions: A Tutorial Review, in: Magnetospheric Current Systems, edited by: Ohtani, S.-I., Fujii, R., Hesse, M., and Lysak, R. L., American Geophysical Union, 91–106, 2000.

Cowley, S. W. H. and Lockwood, M.: Excitation and decay of solar wind-driven flows in the magnetosphere-ionosphere system, Ann. Geophys., 10, 103–115, 1992.

Coxon, J. C., Milan, S. E., Clausen, L. B. N., Anderson, B. J., and Korth, H.: A superposed epoch analysis of the regions 1 and 2 Birkeland currents observed by AMPERE during substorms, J. Geophys. Res.-Space., 119, JA020500, https://doi.org/10.1002/2014JA020500, 2014.

Coxon, J. C., Milan, S. E., Carter, J. A., Clausen, L. B. N., Anderson, B. J., and Korth, H.: Seasonal and diurnal variations in AMPERE observations of the Birkeland currents compared to modeled results, J. Geophys. Res.-Space, 121, JA022050, https://doi.org/10.1002/2015JA022050, 2016.

Erlandson, R. E., Zanetti, L. J., Potemra, T. A., Bythrow, P. F., and Lundin, R.: IMF B_y dependence of region 1 Birkeland currents near noon, J. Geophys. Res.-Space, 93, 9804–9814, https://doi.org/10.1029/JA093iA09p09804, 1988.

Finlay, C. C., Olsen, N., Kotsiaros, S., Gillet, N., and Tøffner-Clausen, L.: Recent geomagnetic secular variation from Swarm and ground observatories as estimated in the CHAOS-6 geomagnetic field model, Earth Planet. Space, 68, 112, 1–18, https://doi.org/10.1186/s40623-016-0486-1, 2016.

Friis-Christensen, E. and Wilhjelm, J.: Polar cap currents for different directions of the interplanetary magnetic field in the Y-Z plane, J. Geophys. Res., 80, 1248–1260, https://doi.org/10.1029/JA080i010p01248, 1975.

Friis-Christensen, E., Kamide, Y., Richmond, A. D., and Matsushita, S.: Interplanetary magnetic field control of high-latitude electric fields and currents determined from Greenland Magnetometer Data, J. Geophys. Res.-Space, 90, 1325–1338, https://doi.org/10.1029/JA090iA02p01325, 1985.

Friis-Christensen, E., Lühr, H., Knudsen, D., and Haagmans, R.: Swarm – An Earth Observation Mission investigating Geospace, Adv. Space Res., 41, 210–216, https://doi.org/10.1016/j.asr.2006.10.008, 2008.

Green, D. L., Waters, C. L., Anderson, B. J., and Korth, H.: Seasonal and interplanetary magnetic field dependence of the field-aligned currents for both Northern and Southern Hemispheres, Ann. Geophys., 27, 1701–1715, https://doi.org/10.5194/angeo-27-1701-2009, 2009.

Guo, J., Liu, H., Feng, X., Pulkkinen, T. I., Tanskanen, E. I., Liu, C., Zhong, D., and Wang, Y.: ML and seasonal dependence of auroral electrojets: IMAGE magnetometer network observations, J. Geophys. Res.-Space, 119, 3179–3188, https://doi.org/10.1002/2014JA019843, 2014.

He, M., Vogt, J., Lühr, H., Sorbalo, E., Blagau, A., Le, G., and Lu, G.: A high-resolution model of field-aligned currents through

empirical orthogonal functions analysis (MFACE), Geophys. Res. Lett., 39, L18105, https://doi.org/10.1029/2012GL053168, 2012.

Huang, C.-S., Sofko, G. J., Koustov, A. V., Andre, D. A., Ruohoniemi, J. M., Greenwald, R. A., and Hairston, M. R.: Evolution of ionospheric multicell convection during northward interplanetary magnetic field with $|B_z/B_y| > 1$, J. Geophys. Res.-Space, 105, 27095–27107, https://doi.org/10.1029/2000JA000163, 2000.

Hughes, T. J. and Rostoker, G.: Current flow in the magnetosphere and ionosphere during periods of moderate activity, J. Geophys. Res., 82, 2271–2282, https://doi.org/10.1029/JA082i016p02271, 1977.

Iijima, T. and Potemra, T. A.: Field-aligned currents in the dayside cusp observed by Triad, J. Geophys. Res., 81, 5971–5979, https://doi.org/10.1029/JA081i034p05971, 1976a.

Iijima, T. and Potemra, T. A.: The amplitude distribution of field-aligned currents at northern high latitudes observed by Triad, J. Geophys. Res., 81, 2165–2174, https://doi.org/10.1029/JA081i013p02165, 1976b.

Iijima, T. and Potemra, T. A.: The relationship between interplanetary quantities and Birkeland current densities, Geophys. Res. Lett., 9, 442–445, https://doi.org/10.1029/GL009i004p00442, 1982.

Iijima, T., Fujii, R., Potemra, T. A., and Saflekos, N. A.: Field-aligned currents in the south polar cusp and their relationship to the interplanetary magnetic field, J. Geophys. Res.-Space, 83, 5595–5603, https://doi.org/10.1029/JA083iA12p05595, 1978.

Juusola, L., Amm, O., Kauristie, K., and Viljanen, A.: A model for estimating the relation between the Hall to Pedersen conductance ratio and ground magnetic data derived from CHAMP satellite statistics, Ann. Geophys., 25, 721–736, https://doi.org/10.5194/angeo-25-721-2007, 2007.

Juusola, L., Milan, S. E., Lester, M., Grocott, A., and Imber, S. M.: Interplanetary magnetic field control of the ionospheric field-aligned current and convection distributions, J. Geophys. Res.-Space, 119, 3130–3149, https://doi.org/10.1002/2013JA019455, 2014.

Kamide, Y. and Akasofu, S.-I.: Global distribution of the Pedersen and Hall Currents and the electric potential pattern during a moderately disturbed period, J. Geophys. Res.-Space, 86, 3665–3668, https://doi.org/10.1029/JA086iA05p03665, 1981.

King, J. H. and Papitashvili, N. E.: Solar wind spatial scales in and comparisons of hourly Wind and ACE plasma and magnetic field data, J. Geophys. Res., 110, A02209, https://doi.org/10.1029/2004JA010804, 2005.

Lühr, H., Rentz, S., Ritter, P., Liu, H., and Häusler, K.: Average thermospheric wind patterns over the polar regions, as observed by CHAMP, Ann. Geophys., 25, 1093–1101, https://doi.org/10.5194/angeo-25-1093-2007, 2007.

Lühr, H., Park, J., Gjerloev, J. W., Rauberg, J., Michaelis, I., Merayo, J. M. G., and Brauer, P.: Field-aligned currents' scale analysis performed with the Swarm constellation, Geophys. Res. Lett., 42, GL062453, https://doi.org/10.1002/2014GL062453, 2015a.

Lühr, H., Kervalishvili, G., Michaelis, I., Rauberg, J., Ritter, P., Park, J., Merayo, J. M. G., and Brauer, P.: The interhemispheric and F region dynamo currents revisited with the Swarm constellation, Geophys. Res. Lett., 42, GL063662, https://doi.org/10.1002/2015GL063662, 2015b.

Macmillan, S. and Olsen, N.: Observatory data and the Swarm mission, Earth Planet. Space, 65, 1355–1362, https://doi.org/10.5047/eps.2013.07.011, 2013.

Moretto, T., Olsen, N., Ritter, P., and Lu, G.: Investigating the auroral electrojets with low altitude polar orbiting satellites, Ann. Geophys., 20, 1049–1061, https://doi.org/10.5194/angeo-20-1049-2002, 2002.

Newell, P. T., Sotirelis, T., Liou, K., Meng, C.-I., and Rich, F. J.: A nearly universal solar wind-magnetosphere coupling function inferred from 10 magnetospheric state variables, J. Geophys. Res.-Space, 112, A01206, https://doi.org/10.1029/2006JA012015, 2007.

Newell, P. T., Sotirelis, T., and Wing, S.: Seasonal variations in diffuse, monoenergetic, and broadband aurora, J. Geophys. Res.-Space, 115, A03216, https://doi.org/10.1029/2009JA014805, 2010.

Olsen, N.: A new tool for determining ionospheric currents from magnetic satellite data, Geophys. Res. Lett., 23, 3635–3638, https://doi.org/10.1029/96GL02896, 1996.

Papitashvili, V. O., Christiansen, F., and Neubert, T.: A new model of field-aligned currents derived from high-precision satellite magnetic field data, Geophys. Res. Lett., 29, 1–4, https://doi.org/10.1029/2001GL014207, 2002.

Richmond, A. D. and Kamide, Y.: Mapping electrodynamic features of the high-latitude ionosphere from localized observations: Technique, J. Geophys. Res.-Space, 93, 5741–5759, https://doi.org/10.1029/JA093iA06p05741, 1988.

Ritter, P., Lühr, H., Viljanen, A., Amm, O., Pulkkinen, A., and Sillanpää, I.: Ionospheric currents estimated simultaneously from CHAMP satelliteand IMAGE ground-based magnetic field measurements: a statisticalstudy at auroral latitudes, Ann. Geophys., 22, 417–430, https://doi.org/10.5194/angeo-22-417-2004, 2004.

Ritter, P., Lühr, H., and Doornbos, E.: Substorm-related thermospheric density and wind disturbances derived from CHAMP observations, Ann. Geophys., 28, 1207–1220, https://doi.org/10.5194/angeo-28-1207-2010, 2010.

Ritter, P., Lühr, H., and Rauberg, J.: Determining field-aligned currents with the Swarm constellation mission, Earth Planet. Space, 65, 1285–1294, https://doi.org/10.5047/eps.2013.09.006, 2013.

Rostoker, G.: Magnetospheric and ionospheric currents in the polar cusp and their dependence on the By component of the interplanetary magnetic field, J. Geophys. Res.-Space, 85, 4167–4176, https://doi.org/10.1029/JA085iA08p04167, 1980.

Senior, C., Robinson, R. M., and Potemra, T. A.: Relationship between field-aligned currents, diffuse auroral precipitation and the westward electrojet in the early morning sector, J. Geophys. Res.-Space, 87, 10469–10477, https://doi.org/10.1029/JA087iA12p10469, 1982.

Siscoe, G. L. and Huang, T. S.: Polar cap inflation and deflation, J. Geophys. Res.-Space, 90, 543–547, https://doi.org/10.1029/JA090iA01p00543, 1985.

Stauning, P.: Field-aligned ionospheric current systems observed from Magsat and Oersted satellites during northward IMF, Geophys. Res. Lett., 29, ORS 6, 4 pp., https://doi.org/10.1029/2001GL013961, 2002.

Tsurutani, B. T. and Gonzalez, W. D.: The efficiency of "viscous interaction" between the solar wind and the magnetosphere during intense northward IMF events, Geophys. Res. Lett., 22, 663–666, https://doi.org/10.1029/95GL00205, 1995.

Vennerstrøm, S., Moretto, T., Olsen, N., Friis-Christensen, E., Stampe, A. M., and Watermann, J. F.: Field-aligned currents in the dayside cusp and polar cap region during northward IMF, J. Geophys. Res.-Space, 107, SMP 18, 5 pp., https://doi.org/10.1029/2001JA009162, 2002.

Wang, H., Lühr, H., and Ma, S. Y.: Solar zenith angle and merging electric field control of field-aligned currents: A statistical study of the Southern Hemisphere, J. Geophys. Res.-Space, 110, A03306, https://doi.org/10.1029/2004JA010530, 2005.

Wang, H., Lühr, H., Ridley, A., Ritter, P., and Yu, Y.: Storm time dynamics of auroral electrojets: CHAMP observation and the Space Weather Modeling Framework comparison, Ann. Geophys., 26, 555–570, https://doi.org/10.5194/angeo-26-555-2008, 2008a.

Wang, H., Ridley, A. J., and Lühr, H.: SWMF simulation of field-aligned currents for a varying northward and duskward IMF with nonzero dipole tilt, Ann. Geophys., 26, 1461–1477, https://doi.org/10.5194/angeo-26-1461-2008, 2008b.

Weimer, D. R.: Maps of ionospheric field-aligned currents as a function of the interplanetary magnetic field derived from Dynamics Explorer 2 data, J. Geophys. Res.-Space, 106, 12889–12902, https://doi.org/10.1029/2000JA000295, 2001.

Wilhjelm, J., Friis-Christensen, E., and Potemra, T. A.: The relationship between ionospheric and field-aligned currents in the dayside cusp, J. Geophys. Res.-Space, 83, 5586–5594, https://doi.org/10.1029/JA083iA12p05586, 1978.

Zhou, Y.-L. and Lühr, H.: Net ionospheric currents closing field-aligned currents in the auroral region: CHAMP results, J. Geophys. Res.-Space, 122, JA023090, https://doi.org/10.1002/2016JA023090, 2017.